

Integration of Chemical and RNAi Multiparametric Profiles Identifies Triggers of Intracellular Mycobacterial Killing

Varadharajan Sundaramurthy,¹ Rico Barsacchi,¹ Nikolay Samusik,¹ Giovanni Marsico,¹ Jerome Gilleron,¹ Inna Kalaidzidis,¹ Felix Meyenhofer,¹ Marc Bickle,¹ Yannis Kalaidzidis,^{1,2} and Marino Zerial^{1,*}

¹Max-Planck Institute of Molecular Cell Biology and Genetics, 108 Pfotenhauerstrasse, 01307 Dresden, Germany

²Belozersky Institute of Physico-Chemical Biology, Moscow State University, 119899 Moscow, Russia

*Correspondence: zerial@mpi-cbg.de

<http://dx.doi.org/10.1016/j.chom.2013.01.008>

SUMMARY

Pharmacological modulators of host-microbial interactions can in principle be identified using high-content screens. However, a severe limitation of this approach is the lack of insights into the mode of action of compounds selected during the primary screen. To overcome this problem, we developed a combined experimental and computational approach. We designed a quantitative multiparametric image-based assay to measure intracellular mycobacteria in primary human macrophages, screened a chemical library containing FDA-approved drugs, and validated three compounds for intracellular killing of *M. tuberculosis*. By integrating the multiparametric profiles of the chemicals with those of siRNAs from a genome-wide survey on endocytosis, we predicted and experimentally verified that two compounds modulate autophagy, whereas the third accelerates endosomal progression. Our findings demonstrate the value of integrating small molecules and genetic screens for identifying cellular mechanisms modulated by chemicals. Furthermore, selective pharmacological modulation of host trafficking pathways can be applied to intracellular pathogens beyond mycobacteria.

INTRODUCTION

Tuberculosis is a disease characterized by an extensive array of interactions between mycobacteria and the host. To maintain their intracellular niche, mycobacteria influence a variety of fundamental host cell processes including apoptosis (Behar et al., 2010; Chen et al., 2006; Keane et al., 2000), autophagy (Gutierrez et al., 2004; Kumar et al., 2010), trafficking (Armstrong and Hart, 1971; Russell, 2001), and signaling (Koul et al., 2004). Therefore, a pharmacological modulation of the host cell mechanisms that are hijacked by the bacteria could, on the one hand, be used to explore the processes altered during the infection and, on the other hand, lead to development of anti-TB compounds.

Exploiting host processes to fight against infectious diseases is currently an underexplored approach. Yet, it presents several advantages. First, the host processes exploited by pathogens are well studied from both a mechanistic and a physiological perspective (Dyer et al., 2008). Second, host kinase and phosphatase inhibitors that kill intracellular mycobacteria have been successfully identified, thus validating the approach (Jayachandran et al., 2007; Jayaswal et al., 2010; Kuijl et al., 2007). Third, it could better prevent the emergence of drug-resistant strains (Schwegmann and Brombacher, 2008). Additionally, critical host cellular responses are conserved across diverse mycobacterial strains, including drug-resistant ones (Kumar et al., 2010). Given the complexity of mycobacteria-host interactions, we reasoned that the target space for perturbations acting upon the host could be significantly larger than so far explored.

Since mycobacteria block phagosome maturation (Armstrong and Hart, 1971; Pieters, 2008; Russell, 2001), a substantial target space could be related to endosomal/phagosomal trafficking. This could be explored by cell-based small molecule screens monitoring intracellular mycobacterial survival. However, a severe constraint is that the primary assay typically does not have the resolution to provide insights into the mode of function of the selected hits (Swinney and Anthony, 2011).

In this study, we addressed this challenge by exploiting our knowledge of the molecular regulation of the endocytic pathway. We recently performed a cell-based genome-wide RNAi screen on endocytosis capturing various features of the endocytic system by quantitative multiparametric image analysis (QMPIA) (Collinet et al., 2010). The QMPIA uncovered general principles governing endocytic trafficking that can also be applied to the analysis of phagosome maturation. Here, we first established a high-content assay to quantify intracellular mycobacterial survival and screened a library of pharmacologically active compounds to identify host-specific modulators. Second, we developed an integrated experimental and computational pipeline to compare the multiparametric profiles from the chemical screen with those from the genome-wide siRNA screen (Collinet et al., 2010). This approach identified chemicals capable of overpowering intracellular mycobacterial survival by modulating the cellular trafficking processes. Our results highlight the value of multiparametric phenotypic analysis to extract functional information from combined chemical and genomic screens.

RESULTS

High-Content Chemical Screen to Identify Modulators of Intracellular Mycobacteria

We developed an integrated experimental and computational strategy for screening, selecting and validating compounds endowed with antimycobacterial activity by acting on the host machinery (Figure 1A). We first established a high-content assay in a human primary macrophage infection model (Experimental Procedures, see the Supplemental Information online). Briefly, cells were infected with *M. bovis* BCG expressing GFP (Dhandayuthapani et al., 1995) and were incubated with chemicals for 48 hr. Since our primary interest was to identify chemical modulators disrupting the host-mycobacteria equilibrium, chemicals were added after the infection. Cells were then fixed and nuclei and cytoplasm stained and imaged using an automated spinning disc confocal microscope. We developed further the QMPIA platform previously used to automatically identify cells, endosomes, and nuclei (Collinet et al., 2010; Rink et al., 2005) by implementing automated algorithms to detect various features of intracellular bacteria and host cell simultaneously (Figure 1B, Supplemental Information). We screened a bioactive library (Microsource Discovery Inc., Spectrum collection, 2,000 compounds) comprising most FDA-approved drugs. The compounds produced reproducible alterations of various parameters such as bacterial number, intensity, and bacterial and host cell morphology (Figure S1A).

We performed cluster analysis using an improvement of the method previously used (Collinet et al., 2010) based on density estimation (N.S., T. Galvez, C. Collinet, G.M., M.Z., and Y.K., unpublished data; Experimental Procedures). The compounds grouped into six distinct clusters, each with a distinct pattern, i.e., phenotypic profile (Figures 1C and 1D, Table S1). The strength of the phenotype is given by its phenoscore. Due to the multiparametric nature of our screening output, we expected each cluster to capture distinct phenotypic features of mycobacteria and the host. Cluster M5 (containing 115 compounds) was of particular interest, as it was characterized by a strong reduction of bacterial parameters but relatively weak changes in host parameters reflecting toxicity, suggesting that the compounds in this cluster are detrimental to bacteria but not significantly toxic to the host.

Since we aimed to identify compounds that act upon the host, we counterselected those directly killing mycobacteria by screening the MSD library using the alamar blue assay (see the Experimental Procedures). Interestingly, only six compounds were shared with cluster M5, suggesting that most compounds in this cluster are not bacteriostatic. Additionally, compounds functionally annotated as “antibacterial” were not enriched in cluster M5 despite scoring in the alamar blue screen (Figure S1B). Standard antimycobacterial drugs were not enriched in any particular cluster and yielded weak phenotypes (Figures S1C–S1F, Supplemental Information). This is probably because our cell-based assay measures the reduction in GFP fluorescence and therefore primarily reflects modulation of lysosomal degradation. Thus, the compounds of cluster M5 could modulate cellular processes at the host-pathogen interface rather than acting directly on the bacteria.

Validation of Three Compounds on *M. tuberculosis*

To validate the results from the screen, we selected three compounds within the cluster M5, namely Nortriptyline, Prochlorperazine edisylate (PE), and Haloperidol (Figures 2B–2D), on the basis of (1) amplitude of the phenotypes (Figure 2E, Figure S2A), showing reduced bacterial intensity, fewer bacteria, and infected cells; and (2) lack of effect in the alamar blue screen. Additionally, these compounds did not show bacteriostatic activity on *M. bovis* BCG-GFP at neutral and acidic pH (Figures S2B and S2C), or plate assay of *M. tuberculosis* (data not shown).

To determine whether the phenotype observed on *M. bovis* BCG-GFP was reproducible on pathogenic *M. tuberculosis*, we performed a colony-forming unit (CFU) assay on *M. tuberculosis* strain H37Rv and two clinical strains using the three selected compounds and the antimycobacterial drugs Rifampin, Rapamycin (Gutierrez et al., 2004), and H89 (Kuijl et al., 2007) as controls. All three selected compounds caused a significant reduction in bacterial colonies in all the strains (Figure 2F), confirming that they impair intracellular survival of *M. tuberculosis*.

Integration of Multiparametric Chemical and Genetic Data Sets to Identify Cellular Processes Modulated by Compounds

Since we aimed to identify compounds restoring mycobacteria-arrested phagosome maturation, we explored the effects of the selected compounds on mycobacterial trafficking. We quantified the colocalization of *M. bovis* BCG-GFP with lysobisphosphatidic acid (LBPA), a marker of late endocytic compartments (Fratti et al., 2001; Kobayashi et al., 1998; see the Experimental Procedures and Figures S2D and S2E). Infected cells treated with the selected compounds showed significantly higher colocalization than control cells (Figure 2G), indicating that the arrest in phagosome maturation was reverted.

A significant challenge in phenotypic chemical screens is to gain insights into the mechanism of action of the selected compounds. Multiparametric profiles are specific signatures of either chemical or genetic perturbations because they capture multiple facets of a biological system. Since random matches between such profiles are unlikely, clues into the molecular processes targeted by the chemicals could be obtained in principle by systematically searching for genetic alterations producing similar phenotypes. Hence, we aimed to match the multiparametric profiles of the compounds from the mycobacteria screen with those of the siRNAs from the genome-wide endocytosis screen (Collinet et al., 2010). However, the two screens are not directly comparable due to their distinct characteristics, i.e., a chemical screen on intracellular mycobacterial survival in human primary macrophages versus a functional genomics screen on endocytosis in HeLa cells. To overcome this problem, we bridged the two data sets via an intermediate screen, where the compounds from cluster M5 were screened on the endocytosis assay in HeLa cells (Figure 3A). HeLa cells were pretreated with the compounds prior to the internalization of fluorescently labeled epidermal growth factor (EGF) and Transferrin (Tfn) for 10 min (Collinet et al., 2010), imaged, and multiple parameters extracted (Supplemental Information).

Density estimation-based clustering separated the compounds into two subclusters, E1 and E2 (Figure 3B, Table S2),

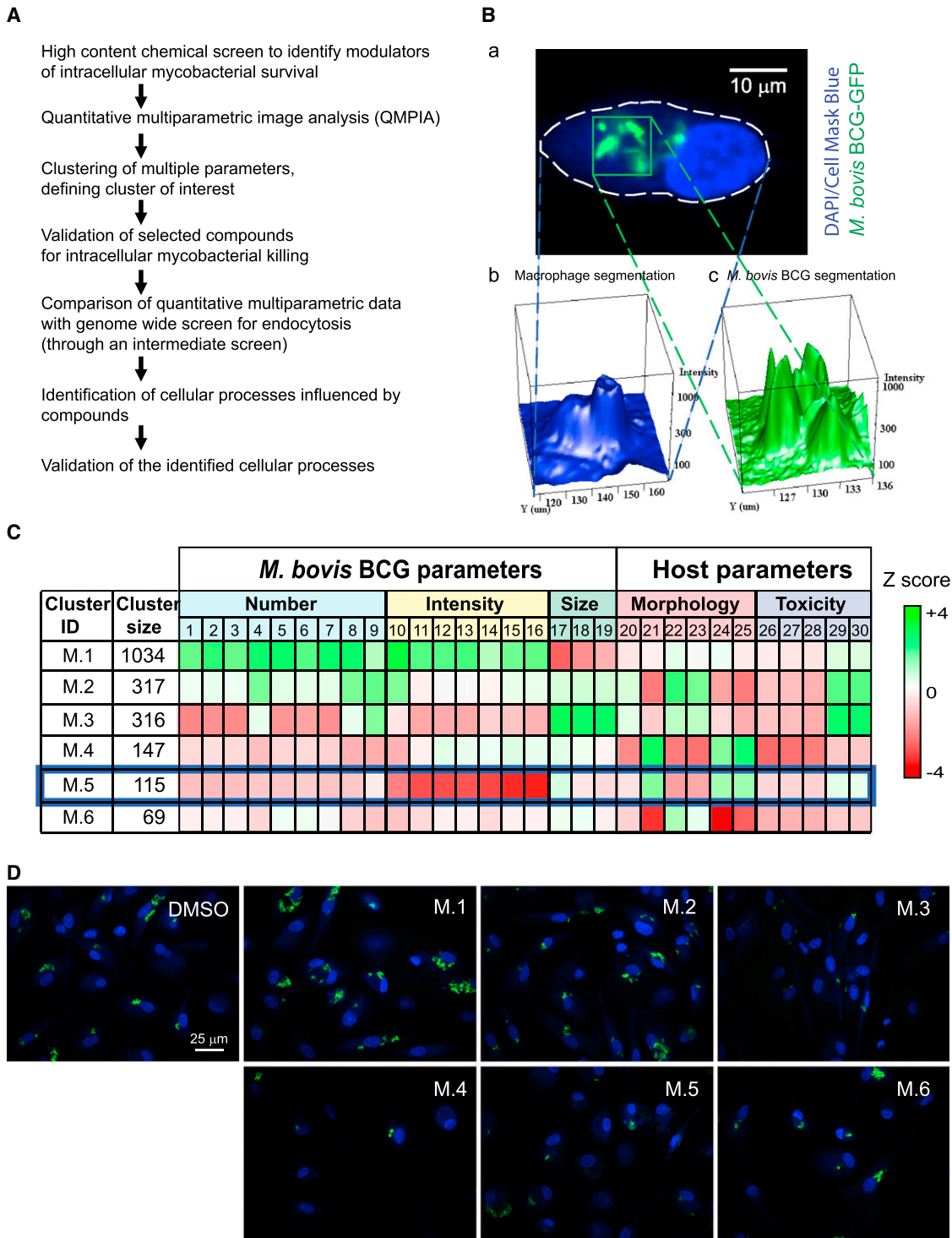


Figure 1. High-Content Image-Based Screen for Intracellular Mycobacteria Survival

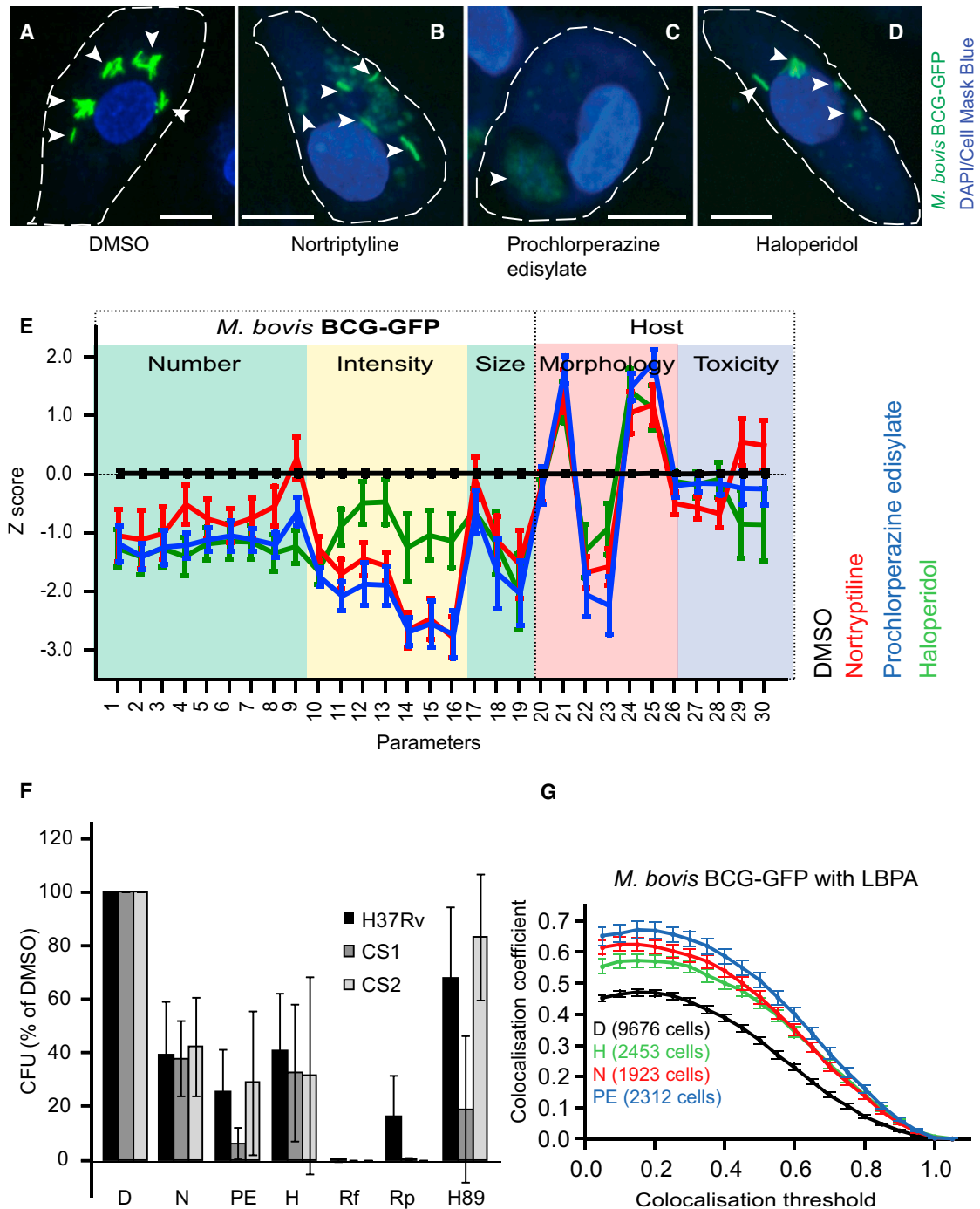
(A) Flowchart of the experimental and computational pipeline used in this study.

(B) (Ba) Representative example of a human primary monocyte-derived macrophage infected with *M. bovis* BCG-GFP with cell contours (dashed line). (Bb) Segmentation of macrophage: intensity distribution of nuclear and cytoplasmic regions used to draw the contours of the cell. (Bc) Segmentation of bacteria: intensity distribution of bacteria in the region marked in the green square used for fitting the bacteria model.

(C) Heatmap representation of the mycobacteria high-content chemical screen after density estimation-based clustering. Rows denote cluster IDs and number of compounds. Columns are parameters of the high-content assay (Supplemental Information). M5 is the cluster analyzed in this study.

(D) Representative images from clusters M1–M6.

See also Figure S1 and Table S1.



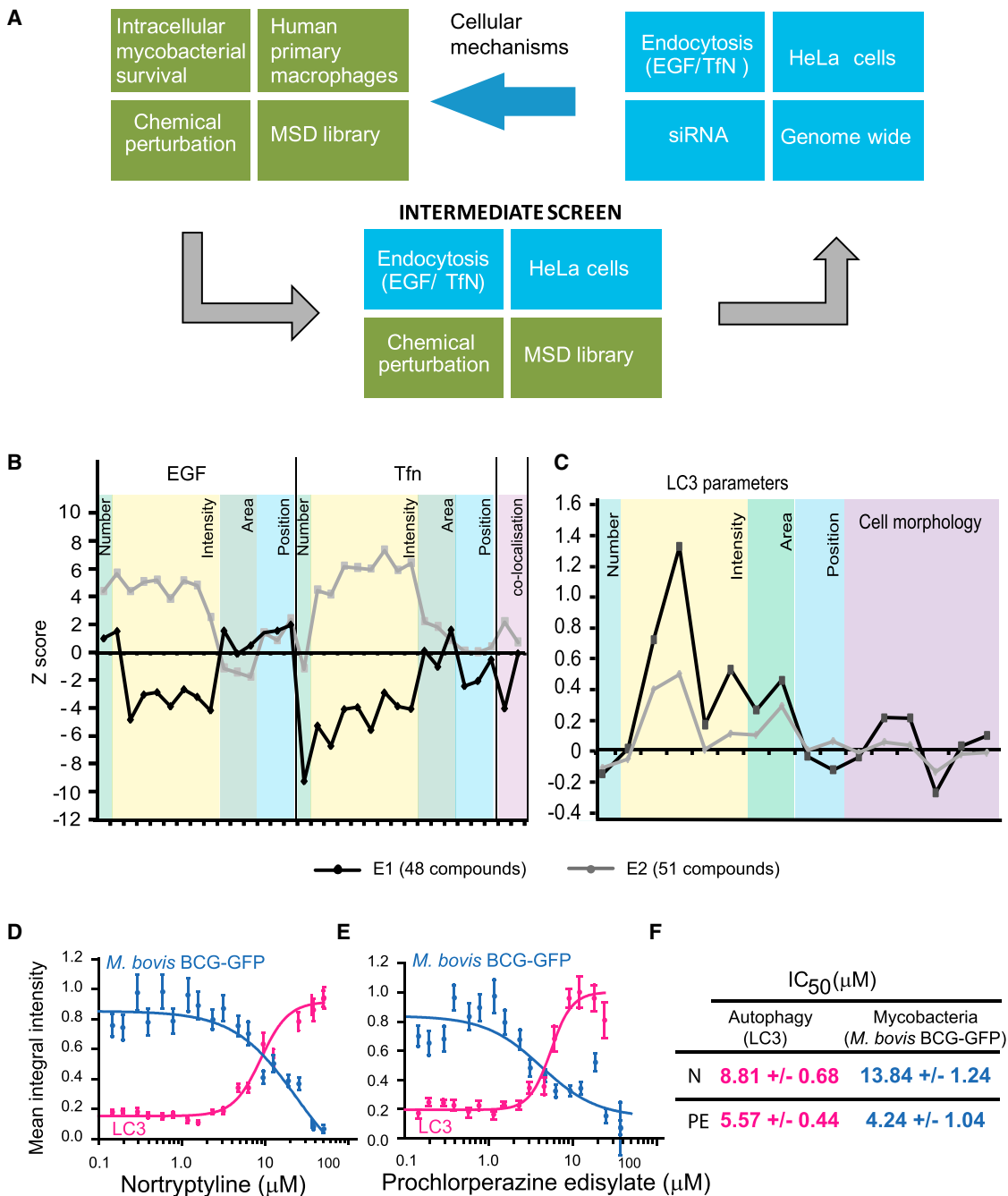


Figure 3. Integration of Chemical and RNAi Screen Data Sets

(A) Scheme illustrating the integration of the primary chemical (green) and RNAi (blue) screen datasets via an intermediate screen on the chemicals from cluster M5.

(B and C) Endocytosis (B) and autophagy(C) profiles of subclusters E1 and E2 from cluster M5. The profiles are average representations of Z scores of the individual compounds within each subcluster. Parameters are grouped into different phenotype classes.

(D and E) Dose-response curves of mean integral intensities of *M. bovis* BCG-GFP (blue) and LC3 (magenta) for Nortryptlyline (D) and prochlorperazine edisylate (E). Error bars are SEM, number of images is 25, data are representative of at least two independent experiments.

(F) Summary of IC₅₀ values calculated from curves in (D) and (E). See also Figure S3, Table S2, and Table S3.

suggesting that the compounds may act by at least two distinct mechanisms. To identify them, we compared the multiparametric profiles of the subclusters E1 and E2 to the genome-wide RNAi screen data set (Collinet et al., 2010) and identified the

sets of genes that are most likely to show similar phenotypes (Experimental Procedures). We computed their representation in KEGG pathways and GO terms (Table S3) and found that “mTOR regulation” and “regulation of autophagy and mTOR”

were significantly enriched in the E1 ($p = 1.2 \times 10^{-4}$ and 9×10^{-4} , respectively) but not the E2 ($p = 0.15$ and 0.4 , respectively) subcluster.

High-Content Autophagy Chemical Screen

Autophagy is a key process regulated by mTOR (Laplanche and Sabatini, 2012) and a known mediator of intracellular mycobacterial survival (Gutierrez et al., 2004; Kumar et al., 2010). The integration approach predicted that compounds from E1 modulate autophagy. To test it, we treated HeLa cells with the compounds, immunostained for the autophagosome marker LC3, and extracted multiple parameters reporting diverse facets of autophagosomes (Supplemental Information). The compounds of subcluster E1, but not E2, had a strong effect on autophagy (Figure 3C, Figure S3A), thus validating the prediction from the integration analysis. Of the three compounds validated in intracellular mycobacterial killing, Nortriptyline and PE belong to subcluster E1, whereas Haloperidol belongs to E2. Consistent with the data of Figure 3C, Nortriptyline and PE, similar to Rapamycin or serum starvation (by HBSS), showed a strong effect on autophagy, whereas Haloperidol did not (Figures S3B and S3C). Human primary macrophages treated with Nortriptyline and PE resembled HeLa cells in showing an increase in both number and integral intensity of LC3 vesicles (Figures S3D and S3E), indicating that their effect of increasing autophagosomes is not cell-type restricted.

To determine whether the accumulation of autophagosomes is related to intracellular mycobacterial killing by Nortriptyline and PE, we first computed their IC_{50} values in the two assays. For both compounds, the IC_{50} values for increased LC3 integral intensity correlated well with decreased *M. bovis* BCG-GFP (Figures 3D–3F), arguing that the two phenotypes are linked. Second, if autophagy modulation were involved in intracellular mycobacterial killing, we should visualize mycobacteria within autophagosomes. To test this, we analyzed mycobacteria-infected cells by electron microscopy. Whereas in control cells mycobacteria resided within single-membrane phagosomes (Figure 4A), cells treated with Nortriptyline and PE clearly showed the presence of mycobacteria within autophagosomes, defined as vesicles containing multiple membrane whorls and delimited by double membrane (Figures 4B–4F). Haloperidol-treated cells, as expected, did not show this effect (Figure S4A). Finally, we tested the effect of an inhibitor of autophagy, 3-methyladenine (3MA) (Seglen and Gordon, 1982). Upon treatment with Nortriptyline and PE in the presence of 3-MA, mycobacteria were observed not in autophagosomes but in phagosomes (Figures S4B–S4D). Additionally, 3-MA reverted the effect of Nortriptyline on mycobacterial survival in both CFU and image-based assays (data not shown), arguing that the effect of the compounds on mycobacteria is related to autophagy.

Nortriptyline and PE Modulate Autophagy by Different Mechanisms

Autophagy is a multistep process consisting of autophagosome formation, maturation, and eventual degradation by fusion with lysosomes (autophagolysosomes). The increase in autophagosomes mediated by Nortriptyline and PE could be due to either a higher rate of formation or a block in maturation and degrada-

tion (autophagic flux) (Klionsky et al., 2008). To distinguish between these possibilities, we used two approaches. First, we tested whether blockers of lysosomal degradation, e.g., inhibitors of acidification (BafilomycinA1 or Chloroquine) that inhibit autophagic flux, had an additive effect with the compounds on autophagosome accumulation (Klionsky et al., 2008). HeLa cells were treated with Nortriptyline and PE in the presence or absence of BafilomycinA1, and LC3 lipidation (LC3-II band) was assessed by immunoblotting. Whereas both Nortriptyline and PE showed significant increase in the LC3-II band, additive effects of BafilomycinA1 were seen only upon Nortriptyline, but not PE, treatment (Figure S5A). In addition, we generated HeLa cells stably expressing LC3 fused to GFP under the control of the endogenous promoter through BAC recombineering (HeLa BAC LC3-GFP; Poser et al., 2008). The results (Figures S5B and S5C) confirmed that Nortriptyline, but not PE, had an additive effect with BafilomycinA1 and Chloroquine in increasing LC3-GFP vesicles.

Second, we used an established assay for measuring autophagic flux based on a tandem mRFP-GFP-LC3 construct (Kimura et al., 2007). Since GFP is quenched in the acidic environment of autophagolysosomes whereas mRFP remains stable, a block in autophagy flux results in higher colocalization of mRFP and GFP compared to induction of autophagy. HeLa cells stably expressing mRFP-GFP-LC3 (Settembre et al., 2011) were treated with the compounds, and the colocalization between mRFP and GFP was quantified. Nortriptyline, similar to starvation-induced autophagy (HBSS), showed a low mRFP to GFP colocalization, whereas PE, similar to BafilomycinA1 and Chloroquine, yielded higher colocalization (Figures 5A and 5B). Similar results were obtained for the colocalization of LC3-GFP with LBPA in HeLa-LC3-GFP cells (Figure S5D). Based on previous studies (Klionsky et al., 2008), these results can be interpreted as indicating that Nortriptyline induces autophagy whereas PE inhibits autophagic flux.

In principle, blockers of autophagy flux should not have a detrimental effect on mycobacteria. Indeed, inhibitors of autophagy flux that abrogate the function of lysosomes by blocking acidification did not affect the intensity of intracellular *M. bovis* BCG-GFP (Figure S5E). In order to determine whether PE has a similar effect on lysosomal pH, we quantified the intensity of the acidotropic dye LysoTracker red over time. Unlike classical blockers of autophagy flux, PE did not have a negative effect on the acidity of lysosomes, but quite the contrary, it significantly increased it (Figure 5C). Moreover, this effect correlated with the presence of mycobacteria within the LysoTracker red-positive vesicles (Figure 5C) and a concomitant reduction in bacterial intensity (Figure 5D).

The increased acidification by PE is in apparent contradiction with the inhibition of autophagic flux. To solve this discrepancy, we treated HeLa cells stably expressing mRFP-GFP-LC3 with the compounds for different periods of time. If autophagy flux were completely blocked, the colocalization between mRFP and GFP (corresponding to nonacidic autophagosomes) should increase with time, whereas if the flux were slowed down, then the colocalization would be expected to decrease (i.e., autophagosomes become acidic). The colocalization of mRFP and GFP increased over time in cells treated with BafilomycinA1 (Figure 5E) or Chloroquine (data not shown). In contrast, in

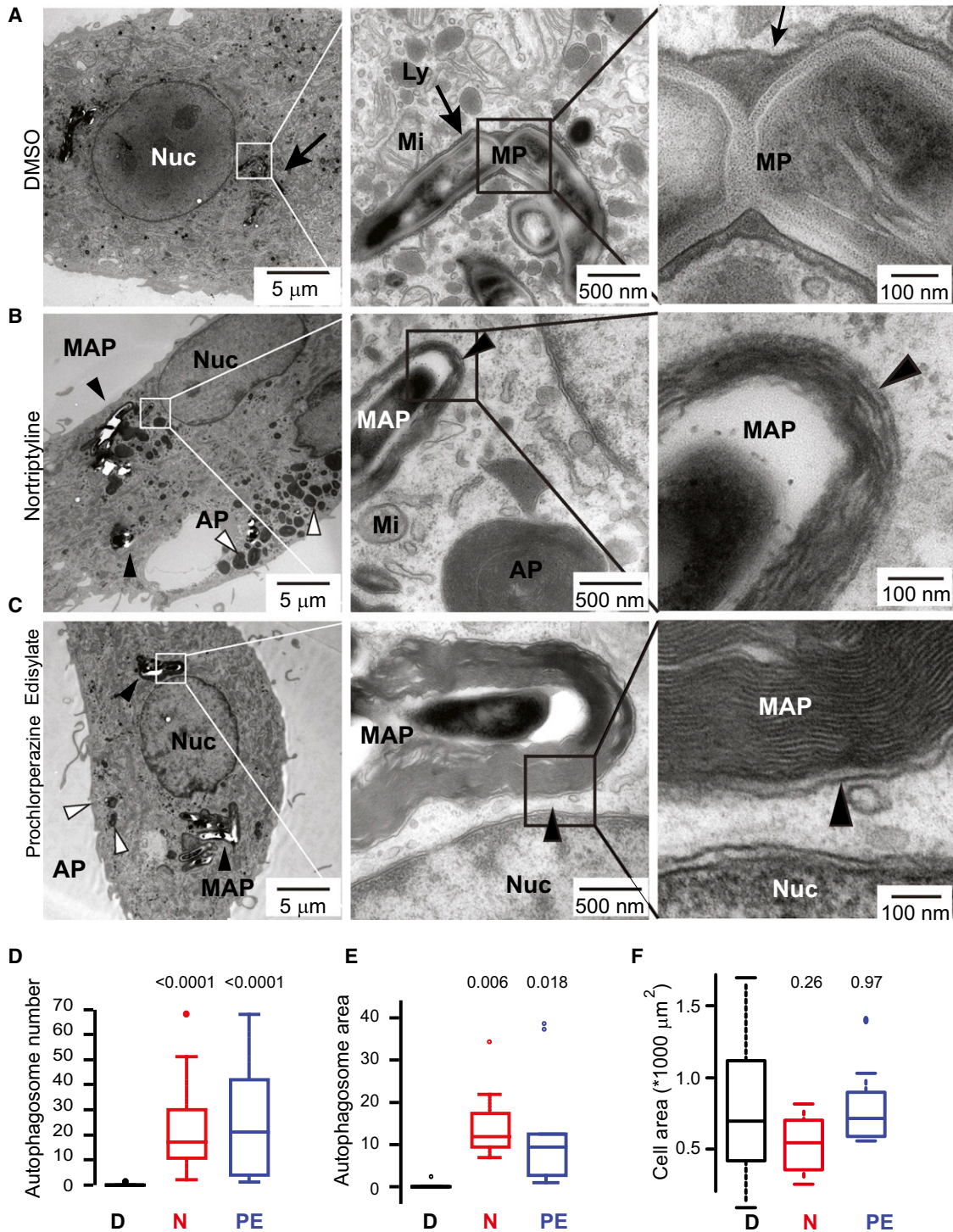


Figure 4. Ultrastructural Analysis of Autophagy and Intracellular Mycobacterial Survival

(A–C) Electron micrographs of *M. bovis* BCG-GFP-infected human primary monocyte-derived macrophages treated with DMSO (A), 10 μM N (B), or PE (C) for 4 hr. Black arrows indicate mycobacterial phagosomes, and black and white arrowheads indicate autophagosomes with and without mycobacteria, respectively. Mitochondria (Mi), nucleus (Nuc), mycobacterial phagosome (MP), autophagosomes (AP), mycobacteria containing autophagosome (MAP).

(D–F) Quantification of number of autophagosomes (D) ($n = 30$), autophagosome area as percentage of total cell area (E) and total cell area (F) ($n = 6$) from the electron micrographs. D (DMSO, 0.01%), N (Nortriptyline, 10 μM), PE (Prochlorperazine edisylate, 10 μM). Numbers denote p values in comparison to DMSO. See also Figure S4.

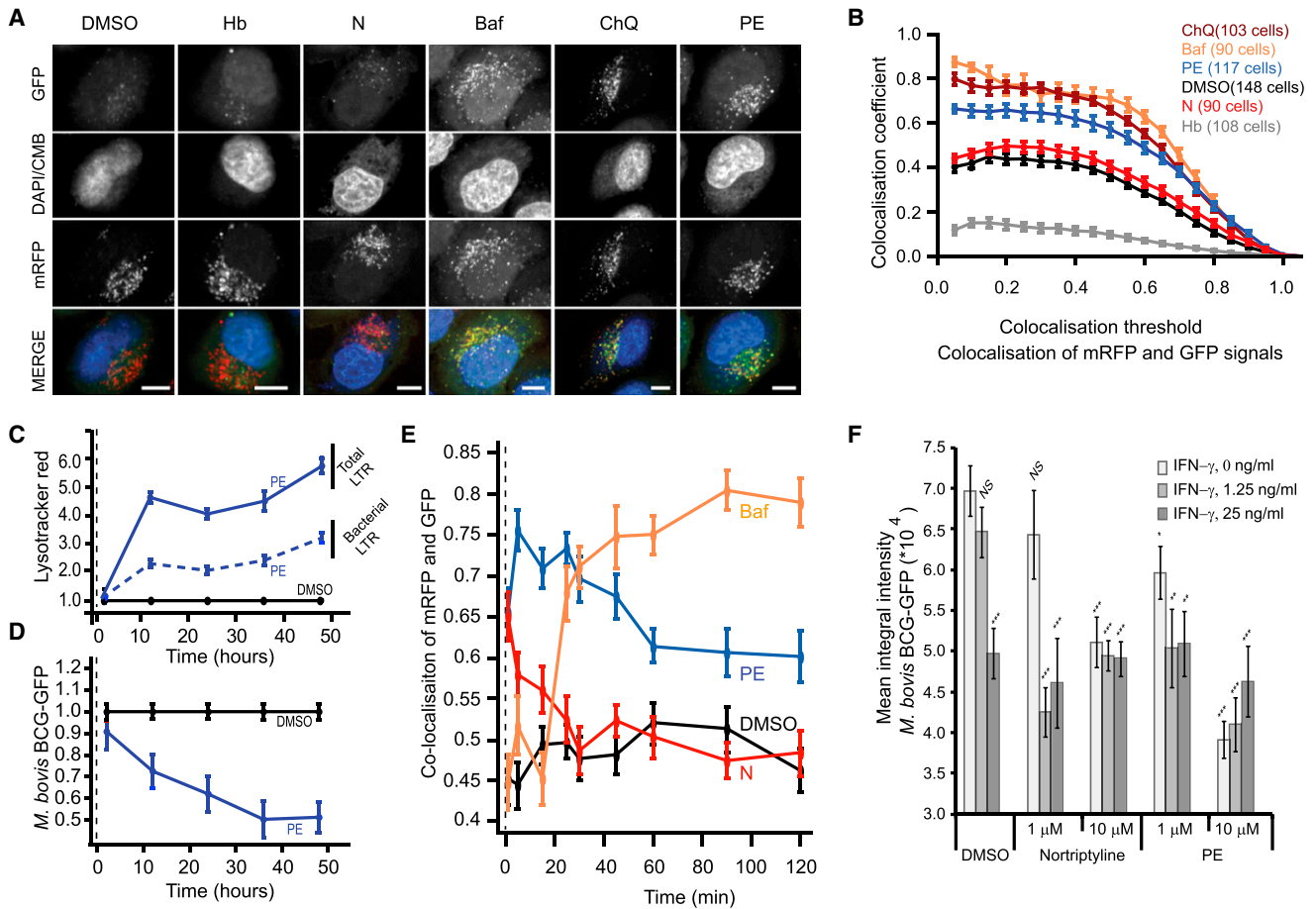


Figure 5. Nortriptyline and PE Modulate Autophagy Differently

(A) Representative images of HeLa cells stably expressing mRFP-GFP-LC3 treated with the indicated chemicals for 2 hr. DAPI/CMB denotes the cell nucleus and cytoplasm. Scale bar, 10 μ m.

(B) Quantification of colocalization between the mRFP and GFP signals. The number of cells analyzed per condition is indicated. Results are representative of four experiments. Error bars are SEM. Abbreviations and concentrations are as in (A).

(C and D) Quantification of integral intensity of lysotracker red-labeled vesicles (C) and *M. bovis* BCG-GFP (D) in infected human primary macrophages treated with either DMSO or PE (10 μ M) for the indicated periods of time. Total and bacterial LTR refer to integral intensity of all acidic compartments and those containing bacteria, respectively. Data are averaged from 45 images/condition/time point and normalized to DMSO to represent fold change (representative of two independent experiments).

(E) Colocalization between the mRFP and GFP signals in HeLa cells stably expressing mRFP-GFP-LC3 treated with the indicated drugs for different periods of time. Colocalization at a single threshold of 0.35 was used to generate the time response curves. Data are from 50 images per condition and from four experiments. For (A), (B), and (E), D (DMSO, 0.01%), Hb (HBSS), N (Nortriptyline, 10 μ M), ChQ (Chloroquine, 25 μ M), Baf (BafilomycinA1, 100 nM), PE (10 μ M).

(F) Mean integral intensity of *M. bovis* BCG-GFP upon treatment of infected human primary macrophages with different concentrations of IFN- γ for 4 hr prior to treatment with either 1 μ M or 10 μ M N or PE, for 48 hr. Significance was calculated by Student's t test. NS $p > 0.05$, * $p < 0.05$, ** $p < 0.001$, *** $p < 0.0001$. Data are averaged from 16 images/condition and are representative of four experiments. For (B)–(F), error bars indicate SEM. See also Figure S5.

PE-treated cells the colocalization increased within the first hour but then progressively decreased (Figure 5E), showing that the autophagosomes acidify over time.

To further characterize the effects of Nortriptyline and PE on autophagy, we tested whether they could synergize with an established physiological inducer of autophagy, Interferon-gamma (IFN- γ) (Gutierrez et al., 2004; Matsuzawa et al., 2012). We preactivated infected cells with IFN- γ and assessed the effect of the compound addition on mycobacterial survival. The results were striking (Figure 5F) and showed that Nortriptyline synergized strongly with IFN- γ , supporting its role in autophagy

induction. PE instead exerted a much weaker effect, providing additional evidence that the two compounds interact differently with the autophagy machinery.

Haloperidol Accelerates Endolysosomal Trafficking

Haloperidol kills intracellular mycobacteria by a mechanism distinct from autophagy. Haloperidol belongs to subcluster E2 (Figure 3B). This subcluster is characterized by a strong alteration of the endocytic profile exemplified by an increase in EGF and Tf α content, increased colocalization of EGF to Tf α (reduced sorting), and accumulation of EGF in large endosomes

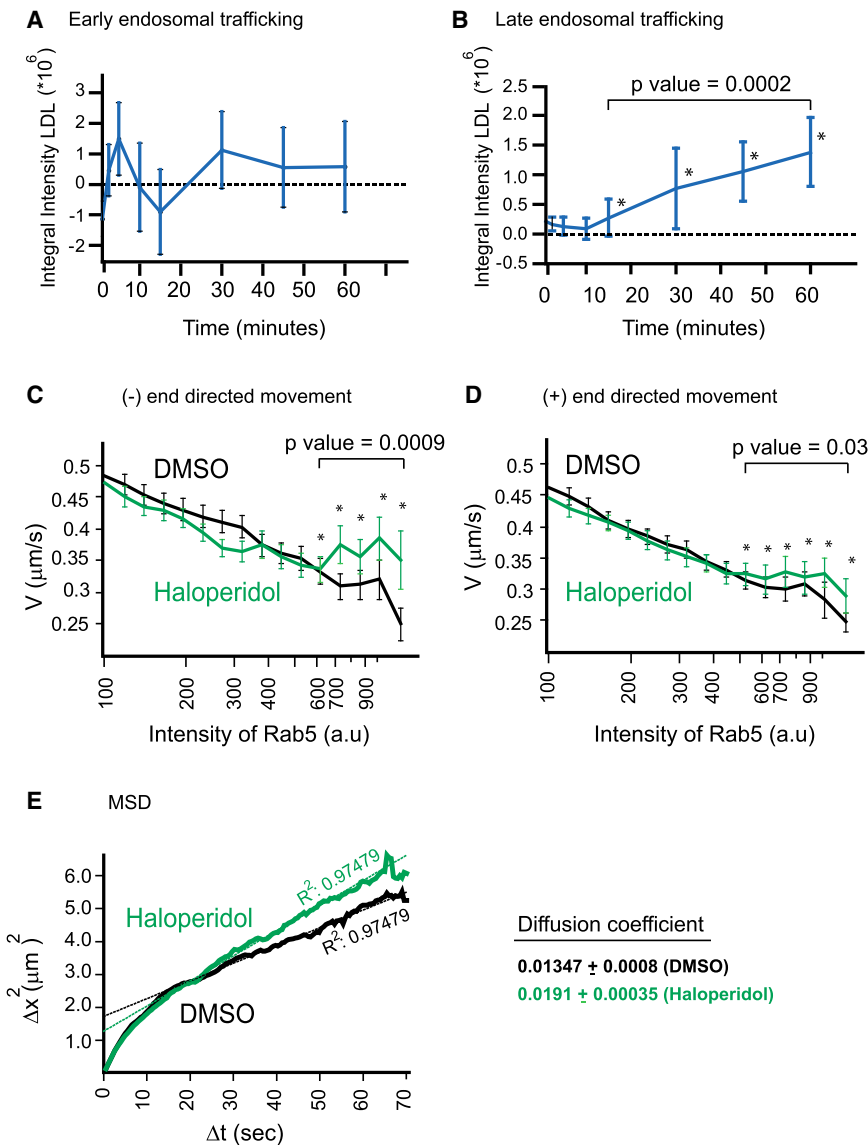


Figure 6. Analysis of Endocytosis Trafficking by Haloperidol

(A and B) The kinetics of endocytic trafficking were quantified using a cell-based LDL trafficking assay. (A) Integral intensity of LDL in early endosomes and (B) late endosomes. Values are H treatment (10 μ M) subtracted from DMSO and derived from an average of 1,200 cells/time point. Error bars are SEM of number of images (average of 40 per condition). Data are representative of two experiments.

(C and D) A431 cells stably expressing Rab5-GFP were treated with either DMSO or Haloperidol (10 μ M) for 2 hr and imaged live. Velocities of minus-end (toward cell center) (C) and plus-end-directed movement (away from cell center) are shown for DMSO-treated cells (black line) and H-treated cells (green line). For curves in (B)–(D), the p value is for points denoted by asterisks (see the [Experimental Procedures](#)). For (C) and (D), error bars are standard deviations, $n = 37$ (DMSO), $n = 29$ (H).

(E) Mean square displacement curves for the movies (Figures 6C and 6D) were computed as described in the [Experimental Procedures](#). The second part of the biphasic curve indicating long timescale movements was fitted using linear least-square fit. Diffusion coefficient is derived from the slope of the fitted curves. See also [Figure S6](#), [Movie S1](#), and [Movie S2](#).

in the cell center. In accordance with the design principles of the endocytic system (Collinet et al., 2010; Rink et al., 2005), the alterations observed argue for a faster degradation. Hence, we hypothesized that Haloperidol could positively modulate endocytic trafficking along the degradative route. To test this hypothesis, we monitored the kinetics of transport of low-density lipoprotein (LDL) from early to late endosomes, using Rab5 (Bucci et al., 1992) and LBPA (Kobayashi et al., 1998) as markers, respectively (Figure S6A). HeLa cells stably expressing GFP-Rab5 from the endogenous promoter (HeLa BAC GFP-Rab5c) (Foret et al., 2012) were treated with Haloperidol and allowed to internalize LDL for different times prior to immunostaining with anti-Apolipoprotein B (ApoB) (to detect LDL) and LBPA antibodies. Haloperidol significantly increased the intensity of LDL in late, but not early, endosomes (Figures 6A and 6B). Similarly, LDL-containing late, but not early, endosomes were larger, more numerous, and closer to the cell center in Haloperidol-treated compared to control cells (Figures S6B–S6G). These

results confirm the prediction that Haloperidol leads to acceleration of trafficking along the degradative pathway.

Phagosome maturation depends on the fusion with early, late endosomes and lysosomes (Desjardins et al., 1994; Fairn and Grinstein, 2012) and is regulated by the motility of endocytic organelles along the cytoskeleton and the recruitment of the membrane tethering fusion machinery. Both processes could be enhanced by Haloperidol. We first

tested the influence of Haloperidol on endosome motility. Increasing concentration of Rab5 and displacement of early endosomes toward cell center are predictive of progression from early to late endosomes (Del Conte-Zerial et al., 2008; Rink et al., 2005). We therefore quantified endosome motility in cells stably expressing GFP-Rab5, as previously described (Rink et al., 2005) (Movie S1 and Movie S2), and computed the velocity toward the cell center (minus end microtubule directed) and periphery (plus end) as a function of GFP-Rab5 intensity. Haloperidol-treated cells showed a much higher motility of early endosomes harboring high levels of Rab5, and this enhancement was higher toward the cell center (Figures 6C and 6D). Next, we computed the mean square displacement of endosomes over time, an established way to characterize motility patterns (Caspi et al., 2002). In Haloperidol-treated cells, long, but not short, timescale movements of GFP-Rab5 endosomes were significantly accelerated (Figure 6E). Thus, Haloperidol accelerates the centripetal movement of early endosomes.

Diffusion coefficient
 0.01347 ± 0.0008 (DMSO)
 0.0191 ± 0.00035 (Haloperidol)

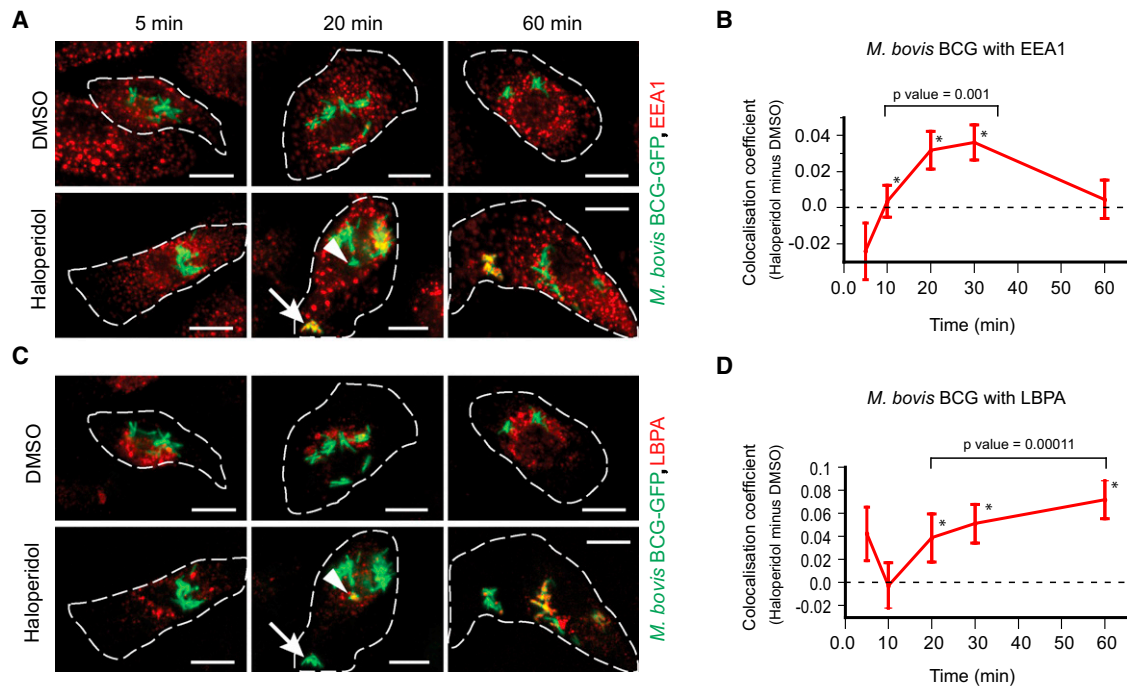


Figure 7. Haloperidol Induces Alterations in Intracellular Mycobacterial Trafficking

(A and C) Representative images of *M. bovis* BCG-GFP-infected human primary macrophages treated with 10 μ M Haloperidol for the indicated times and immunostained for EEA1 (A) and LBPA (C). The outline of infected cells is shown in dashed lines. Scale bar, 10 μ m. The presence of EEA1 and LBPA on mycobacterial phagosome, as indicated by arrows and arrowheads (at 20 min), respectively, is mutually exclusive. (B and D) Quantification of colocalization of *M. bovis* BCG-GFP with EEA1 (B) and LBPA (D). A stringency threshold of 0.35 was used. Data are averaged from about 1,000 infected cells and are representative of at least two independent experiments. Error bars are SEM. The p value denotes significance for the consecutive points of the time series denoted by asterisks (see the [Experimental Procedures](#)).

Second, we tested whether Haloperidol could lead to increased delivery of the membrane-tethering and fusion machinery to the arrested mycobacterial phagosome. Mycobacterial phagosomes contain Rab5, but not Rab7 (Alix et al., 2011; Russell, 2001), and lack PI(3)P (Vergne et al., 2005), which mediates the recruitment of various Rab5 effectors, including the membrane-tethering factor early endosomal antigen 1 (EEA1) (Christoforidis et al., 1999). Therefore, mycobacterial phagosomes lack EEA1 (Fratti et al., 2001). If Haloperidol could restore such machinery, one would expect to see a small, transient increase in EEA1 on mycobacterial phagosomes. We treated *M. bovis* BCG-infected cells with Haloperidol for different times and quantified the colocalization of mycobacteria with EEA1 and LBPA. Whereas in control cells, as expected, mycobacterial phagosomes were devoid of EEA1 at all times (Figure 7A, upper panels; Figure 7B), in Haloperidol-treated cells a small but significant fraction of EEA1 localized to mycobacterial phagosomes 20–30 min posttreatment (Figure 7A, lower panels; Figure 7B). Such an effect was specific for Haloperidol, as it was not observed in cells treated with Nortriptyline and PE (data not shown). Moreover, in Haloperidol-treated cells the colocalization of mycobacteria and LBPA increased with time (Figures 7C and 7D). Altogether, these data indicate that Haloperidol restores the delivery of critical components of the membrane-tethering machinery to the mycobacterial phagosomes, thereby delivering mycobacteria to lysosomes.

DISCUSSION

In this study, we developed a pipeline of experimental and computational methods to identify pharmacological modulators of host cellular processes that trigger killing of intracellular mycobacteria. First, we established a multiparametric image-based assay to quantify mycobacterial survival in human primary macrophages. Second, we used a pharmacological approach to disrupt the host-pathogen equilibrium in favor of the host. Third, we developed computational methods to compare the multiparametric profiles of chemicals with those of siRNAs, to identify the cellular mechanisms underlying the antibacterial activities of the compounds. Fourth, we validated the predictions from such comparison on the three selected compounds and established that two of them modulate autophagy via distinct mechanisms and the third one accelerates endocytic trafficking. Our results demonstrate the predictive value of comparing quantitative multiparametric profiles from chemical and genetic screens to decipher the cellular mechanisms of chemical action. They further show that trafficking pathways can be modulated pharmacologically to stimulate intracellular mycobacteria killing.

The key feature of our intracellular mycobacterial survival assay is the multiplicity and reliability of parameters capturing various features of bacteria and host at high resolution. Interestingly, most compounds in the selected hit cluster (M5) are not directly antimycobacterial. Although we cannot rule out completely the possibility that the compounds may kill bacteria

directly within infected cells, we favor the interpretation that they act by modulating the host for the following reasons. First, the M5 cluster showed very little overlap with the compounds which act directly on bacteria. Second, the three selected compounds do not kill mycobacteria outside the host cell under the different conditions tested. Third, they show similar effects on uninfected cells. Fourth, the effect of Nortriptyline and PE can be reverted by inhibiting a host cellular process (autophagy). Fifth, Nortriptyline showed strong phenotypic correlation with a structural analog, Amitriptyline, in mycobacteria as well as endocytosis and autophagy screens. Here, only structural analogs having a Tanimoto distance >0.9 were considered (Supplemental Information and Figures S2F–S2I). Sixth, Nortriptyline and PE enhance the acidity of lysosomes. This correlates with delivery of mycobacteria to lysosomes and their survival. Additionally, standard antimycobacterial drugs showed weaker phenotypes compared to the selected compounds. Most likely, this is because our assay measures GFP fluorescence from mycobacteria that decays at different rates, depending on whether the host degradation machinery can be accelerated or not. In support of this, Rifampicin did not show enhanced lysosomal acidity. Thus, our screening platform has a bias for compounds that boost host mechanisms. Importantly, our data argue that such compounds are likely to be missed in a screen for antimycobacterial compounds outside the context of infected cells.

Whereas cell-based high-content screens have several advantages over traditional target-based HT screens, understanding the mechanism of action of the identified compounds is a critical bottleneck (Swinney and Anthony, 2011). One possible approach is to identify genes that when silenced produce a phenotype similar to that of small inhibitory molecules (Eggert et al., 2004). However, there are significant caveats to this approach: for example, small molecules usually act rapidly, whereas RNAi is gradual and requires longer times, possibly allowing the system to adapt to a new steady state. Moreover, the biological activity of small molecules may result from the modulation of multiple targets (Imming et al., 2006) rather than specific ones as in RNAi, excluding off-target effects. We reasoned that although it may prove difficult to identify targets of small molecules by comparing the phenotypic profiles of chemicals and silenced genes, this approach may nevertheless allow the identification of the cellular pathways affected, as long as the phenotypes are described with sufficient detail and specificity. Therefore, we captured the phenotypes through QMPIA, and, by integrating chemical and functional genomics data sets, we differentiated hit compounds of the mycobacteria screen into distinct groups on the basis of their phenotypes on endocytosis. Using this strategy, we could show both computationally and experimentally that one of the groups is significantly enriched for modulators of autophagy, a well-known antimycobacterial cell-defense mechanism (Gutierrez et al., 2004; Kumar et al., 2010). Remarkably, autophagy phenotypes could thus be identified using a general endocytosis assay.

Nortriptyline and PE influence autophagy differently. Whereas Nortriptyline induces the formation of autophagosomes, PE slows down autophagic flux. The basal rate of autophagy may be sufficient to accumulate autophagosomes in the presence of PE. These autophagosomes progressively acidify over time and become competent for mycobacteria degradation (Ponpuak

et al., 2010). PE may act at different stages, e.g., on the fusion with lysosomes. Detailed characterization of the interactions of Nortriptyline and PE with the autophagy machinery will lead to a more precise understanding of their mode of action.

The identification of Haloperidol as an antimycobacterial compound provides proof of principle for the pharmacological modulation of endocytic trafficking as a means of boosting the host defense system to clear intracellular pathogens. Most importantly, our data imply that such an approach is feasible without inducing overt toxicity to cells. Haloperidol leads to faster degradation of cargo by accelerating transport from early to late endocytic compartments. Previous work has identified both general design principles and molecular details of the machinery underlying endosome biogenesis and progression that are relevant to the pharmacological properties of Haloperidol. First, transport of cargo (LDL) along the degradative route entails a conversion from Rab5- to Rab7-positive endosomes (Rink et al., 2005). Such conversion is based on a cut-out switch (Del Conte-Zerial et al., 2008) that requires the endosomal levels of Rab5 to pass a threshold value prior to triggering a feedback loop causing its removal and substitution with Rab7. Second, our recent systems survey on endocytosis has revealed that the centripetal movement of endosomes previously observed by quantitative live-cell imaging (Rink et al., 2005) is a master parameter that regulates several other properties of the early endosome network, including cargo progression (Collinet et al., 2010). Mycobacterium interferes with such a switch, keeping the phagosome in an arrested state. Remarkably, Haloperidol exerts a positive influence on both centripetal movement of endosomes and membrane recruitment of the Rab5 machinery. By shifting the molecular composition of the mycobacterial phagosome, Haloperidol counteracts the fine balance between phagosome activity and maturation arrest, restoring maturation. Thus, relatively subtle alterations in the general endocytic trafficking machinery are sufficient to cause dramatic effects on intracellular mycobacterial survival.

Our results revealed antimycobacterial properties for three existing drugs. While Nortriptyline is an antidepressant, PE and Haloperidol are antipsychotics. The serum concentrations achieved in patients for these drugs are lower than the in vitro antibacterial IC₅₀ (Regenthal et al., 1999). In principle, they would have to be made significantly more potent or achieve significantly higher serum levels to be effective in antimycobacterial therapy. However, it is difficult to compare the effectiveness of the drugs under the particular conditions used in vitro with their pharmacokinetics properties in patients, and further studies are necessary to corroborate their antimycobacterial activity in vivo. Nevertheless, our work demonstrates that it is possible to find existing compounds with previously unrecognized antimycobacterial activity and mode of action. Interestingly, PE is also used as antiemetic and administered in patients with MDR-TB to alleviate ancillary symptoms of nausea and vomiting (Shubin et al., 1958). The finding that three neuromodulators are endowed with membrane trafficking and antimycobacterial activity suggests that compounds can exert diverse biological effects depending on the cellular context analyzed. Such influences are typically neglected in target-based screenings. Repurposing existing drugs for additional applications could thus open new avenues and lead to rapid therapeutic advances (Huang et al.,

2011). However, it is not excluded that the effects on intracellular transport highlighted in this study may even be part of the mechanism of action of the compounds in neuromodulation. The mechanistic clues obtained here open the possibility of exploring the role of cellular processes, i.e., autophagy and modulation of endocytic trafficking, in the context of their original therapeutic use. Indeed, many tricyclic antidepressants, regarded as mediators of neurotransmitter signaling, show significant effects on autophagy (Rossi et al., 2009; Zschocke et al., 2011). Synergistic activities of such compounds with other antibacterial and immune modulators, such as IFN- γ , could be exploited to yield more potent pharmacological interventions. Finally, the methods described here can be adapted to other diseases where host cell processes need to be targeted. The compounds identified may therefore also be effective against pathogens using similar survival strategies.

EXPERIMENTAL PROCEDURES

High-Content Screen for Intracellular Mycobacteria Survival

Human primary monocyte-derived macrophages were infected with *M. bovis* BCG-GFP for 1 hr at moi of 1:10, washed extensively (Biotec EL406). After adding the compounds (10 μ M) (Beckman FxP automatic workstation), cells were incubated for 48 hr, fixed with 3.7% PFA (Sigma), stained with 1 μ g/ml DAPI and 3 μ g/ml Cell Mask Blue (Invitrogen), and imaged using the automated spinning disk confocal Opera (Perkin Elmer). See the [Supplemental Information](#) for details.

Data Analysis: Density-Based Clustering

Multiparametric profiles from the chemical screen were clustered using density-based clustering algorithm with von Mises-Fisher kernel used for density estimate (N.S., T. Galvez, C. Collinet, G.M., M.Z., and Y.K., unpublished data). Clustering was performed varying the kernel concentration parameter k . For every data set, the number of clusters obtained stabilized within a k range of 10–150. Further increase of k would not lead to an increase in the number of clusters. For each data set, a cluster was manually selected at the first value of k that produced clusters that were stable in number and size. k values for the mycobacteria and endocytosis screens were 30 and 90, respectively.

Integrating Chemical and Genetic Screens

Representative profiles of the two endocytosis subclusters were generated by averaging the profiles of individual compounds in each subcluster. For these two profiles, we assembled a list of genes from the endocytosis screen (Collinet et al., 2010) that had a Phenoscore >0.95 and a Pearson correlation of 0.7. These lists were subjected to gene annotation enrichment analysis using a standard hypergeometric test. Gene annotations were obtained from Gene Ontology and KEGG Pathway databases.

Intracellular Mycobacterial Trafficking Assay

Human primary monocyte-derived macrophages were infected with *M. bovis* BCG-GFP and stained for lysotracker red or LBPA as markers of late endosomes and lysosomes (Kobayashi et al., 1998; Schmid and Cullis, 1998). Colocalizations were scored over a range of stringency thresholds varying from 0 (most relaxed) to 1 (most stringent).

Alamar Blue Screen for Antibacterial Compounds

To mid-log phase *M. bovis* BCG-GFP seeded into 384-well plates (OD₆₀₀ = 0.03) in a volume of 90 μ l 7H9, compounds were added to a final concentration of 10 μ M. DMSO and Amikacin (200 μ g/ml) were included as negative and positive controls, respectively. Plates were incubated at 37°C for 4 days, followed by addition of 10 μ l of 1:1 mix of alamar blue (serotec) and 10% Tween-80. After 24 hr at 37°C, fluorescence was read in the Tecan Pro (Ex 535 nm; Em 590 nm). Analysis was done per plate. Compounds with a Z

score >3 were considered hits. The screen was repeated twice (Z' factors are 0.85 and 0.9 for each run). Hits from both runs were combined.

High-Content Autophagy Assay

HeLa cells were treated with the compounds at a final concentration of 10 μ M, incubated for 4 hr, fixed with 3.7% PFA, and immunostained with anti-LC3 antibody (clone PM036, MBL Labs). Cells were counterstained by DAPI and Cell Mask blue, imaged, and analyzed as described above.

Dose-Response Curves

To calculate IC₅₀ for mycobacterial survival, human primary monocyte-derived macrophages were infected with *M. bovis* BCG-GFP, treated with different concentrations of the compounds for 48 hr, and fixed. For autophagy assay, the same preparation of cells was treated with the compounds for 2 hr, fixed, and immunostained for LC3. Cells were imaged and analyzed as described.

M. tuberculosis CFU Assay

Human primary macrophages were infected with virulent *M. tuberculosis* strain H37Rv and two different clinical isolates (CS1 and CS2) for 1 hr at moi 1:10, washed, treated with Amikacin (200 μ g/ml) for 45 min, washed again, and treated with the compounds. Cells were lysed after 48 hr with 0.05% SDS and plated in multiple dilutions on 7H11 agar plates. Colonies were counted after incubation at 37°C for 3 weeks.

Electron Microscopy

Cells were fixed with 2.5% glutaraldehyde followed by postfixation in ferrocyanide-reduced osmium following standard protocols (Karnovsky, 1971) and embedded with epon. Then 70 nm thin sections were cut on a Leica ultramicrotome, stained with uranyl acetate and lead citrate following classical procedures, and imaged on a 100 kV Tecnai 12 TEM microscope. For area measurements, several overlapping high-magnification images covering the whole cell were acquired, and a montage was generated using ImageJ.

Live-Cell Imaging

A431 cells stably expressing GFP-Rab5 were treated with 10 μ M Haloperidol for 2 hr and imaged live using Zeiss Duo scan microscope at 0.098 s/frame for 2 min. Individual endosomes were identified and tracked over time as described (Rink et al., 2005). To calculate mean square displacement, endosomal tracks were first iteratively divided into nonoverlapping equal time intervals from 0.1 to 70 s, and their displacements were computed for each interval. Next, the square of displacement for all endosomal tracks for a given condition was averaged and plotted as a function of the time interval. In such a curve, early endosomes show a characteristic biphasic behavior, which we refer to as short timescale and long timescale movements.

Estimation of p Value for Time Series

The null hypothesis tested is that deviation of a sequence of N measurements from zero is the result of normally distributed noise. Given that every measurement i in the series has a value Δ_i and variance σ_i^2 , we computed the probability of the null hypothesis (p value) as

$$p_{\text{value}} = \frac{1}{2} \left(1 - \operatorname{erf} \left(\frac{1}{\sqrt{2}} \left(\frac{\sum_{i=1}^N \Delta_i}{\sum_{i=1}^N \sigma_i^2} \right)^2 \right) \right)$$

SUPPLEMENTAL INFORMATION

Supplemental Information includes six figures, two movies, three tables, Supplemental Experimental Procedures, and Supplemental References and can be found with this article at <http://dx.doi.org/10.1016/j.chom.2013.01.008>.

ACKNOWLEDGMENTS

We thank Dr. J. Pieters (Biozentrum, University of Basel) for *M. bovis* BCG-GFP strain, Dr. J. Gruenberg (University of Geneva) for anti-LBPA antibody, Drs. A. Ballabio and D. Medina (TIGEM, Naples) for HeLa mRFP-GFP-LC3 stable

clone, Drs. E. Jacobs and S. Monecke (TU, Dresden) for providing *M. tuberculosis* strains, and Dr. E. Fava (DKNZ, Bonn) for the initial work. We are indebted to N. Tomschke, M. Stoeter, A. Giner, S. Seifert, C. Moebius, C. Andree, and the HT-TDS for expert technical assistance; I. Poser and BAC recombinering facility for HeLa LC3-GFP BAC and HeLa Rab5-GFP BAC cell lines; the High-Performance Computing Center at TUD, M. Chernykh, and the computer department for expert IT assistance; and E. Perini, M. McShane, and K. Simons for critical comments on the manuscript. This work was supported by EU-FP7-funded projects NATT, PHAGOSYS, APO-SYS, and the Max-Planck Society.

Received: August 2, 2012

Revised: November 2, 2012

Accepted: January 3, 2013

Published: February 13, 2013

REFERENCES

- Alix, E., Mukherjee, S., and Roy, C.R. (2011). Subversion of membrane transport pathways by vacuolar pathogens. *J. Cell Biol.* **195**, 943–952.
- Armstrong, J.A., and Hart, P.D. (1971). Response of cultured macrophages to *Mycobacterium tuberculosis*, with observations on fusion of lysosomes with phagosomes. *J. Exp. Med.* **134**, 713–740.
- Behar, S.M., Divangahi, M., and Remold, H.G. (2010). Evasion of innate immunity by *Mycobacterium tuberculosis*: is death an exit strategy? *Nat. Rev. Microbiol.* **8**, 668–674.
- Bucci, C., Parton, R.G., Mather, I.H., Stunnenberg, H., Simons, K., Hoflack, B., and Zerial, M. (1992). The small GTPase rab5 functions as a regulatory factor in the early endocytic pathway. *Cell* **70**, 715–728.
- Caspi, A., Granek, R., and Elbaum, M. (2002). Diffusion and directed motion in cellular transport. *Phys. Rev. E Stat. Nonlin. Soft Matter Phys.* **66**, 011916. <http://dx.doi.org/10.1103/PhysRevE.66.011916>.
- Chen, M., Gan, H., and Remold, H.G. (2006). A mechanism of virulence: virulent *Mycobacterium tuberculosis* strain H37Rv, but not attenuated H37Ra, causes significant mitochondrial inner membrane disruption in macrophages leading to necrosis. *J. Immunol.* **176**, 3707–3716.
- Christoforidis, S., McBride, H.M., Burgoyne, R.D., and Zerial, M. (1999). The Rab5 effector EEA1 is a core component of endosome docking. *Nature* **397**, 621–625.
- Collinet, C., Stöter, M., Bradshaw, C.R., Samusik, N., Rink, J.C., Kenski, D., Habermann, B., Buchholz, F., Henschel, R., Mueller, M.S., et al. (2010). Systems survey of endocytosis by multiparametric image analysis. *Nature* **464**, 243–249.
- Del Conte-Zerial, P., Bruschi, L., Rink, J.C., Collinet, C., Kalaidzidis, Y., Zerial, M., and Deutsch, A. (2008). Membrane identity and GTPase cascades regulated by toggle and cut-out switches. *Mol. Syst. Biol.* **4**, 206. <http://dx.doi.org/10.1038/msb.2008.45>.
- Desjardins, M., Huber, L.A., Parton, R.G., and Griffiths, G. (1994). Biogenesis of phagolysosomes proceeds through a sequential series of interactions with the endocytic apparatus. *J. Cell Biol.* **124**, 677–688.
- Dhandayuthapani, S., Via, L.E., Thomas, C.A., Horowitz, P.M., Deretic, D., and Deretic, V. (1995). Green fluorescent protein as a marker for gene expression and cell biology of mycobacterial interactions with macrophages. *Mol. Microbiol.* **17**, 901–912.
- Dyer, M.D., Murali, T.M., and Sobral, B.W. (2008). The landscape of human proteins interacting with viruses and other pathogens. *PLoS Pathog.* **4**, e32. <http://dx.doi.org/10.1371/journal.ppat.0040032>.
- Eggert, U.S., Kiger, A.A., Richter, C., Perlman, Z.E., Perrimon, N., Mitchison, T.J., and Field, C.M. (2004). Parallel chemical genetic and genome-wide RNAi screens identify cytokinesis inhibitors and targets. *PLoS Biol.* **2**, e379. <http://dx.doi.org/10.1371/journal.pbio.0020379>.
- Fairn, G.D., and Grinstein, S. (2012). How nascent phagosomes mature to become phagolysosomes. *Trends Immunol.* **33**, 397–405.
- Foret, L., Dawson, J.E., Villaseñor, R., Collinet, C., Deutsch, A., Bruschi, L., Zerial, M., Kalaidzidis, Y., and Jülicher, F. (2012). A general theoretical framework to infer endosomal network dynamics from quantitative image analysis. *Curr. Biol.* **22**, 1381–1390.
- Fratti, R.A., Backer, J.M., Gruenberg, J., Corvera, S., and Deretic, V. (2001). Role of phosphatidylinositol 3-kinase and Rab5 effectors in phagosomal biogenesis and mycobacterial phagosome maturation arrest. *J. Cell Biol.* **154**, 631–644.
- Gutierrez, M.G., Master, S.S., Singh, S.B., Taylor, G.A., Colombo, M.I., and Deretic, V. (2004). Autophagy is a defense mechanism inhibiting BCG and *Mycobacterium tuberculosis* survival in infected macrophages. *Cell* **119**, 753–766.
- Huang, R., Southall, N., Wang, Y., Yasgar, A., Shinn, P., Jadhav, A., Nguyen, D.T., and Austin, C.P. (2011). The NCGC pharmaceutical collection: a comprehensive resource of clinically approved drugs enabling repurposing and chemical genomics. *Sci. Transl. Med.* **3**. <http://dx.doi.org/10.1126/scitranslmed.3001862>, 80ps16.
- Imming, P., Sinning, C., and Meyer, A. (2006). Drugs, their targets and the nature and number of drug targets. *Nat. Rev. Drug Discov.* **5**, 821–834.
- Jayachandran, R., Sundaramurthy, V., Combaluzier, B., Mueller, P., Korf, H., Huygen, K., Miyazaki, T., Albrecht, I., Massner, J., and Pieters, J. (2007). Survival of mycobacteria in macrophages is mediated by coronin 1-dependent activation of calcineurin. *Cell* **130**, 37–50.
- Jayaswal, S., Kamal, M.A., Dua, R., Gupta, S., Majumdar, T., Das, G., Kumar, D., and Rao, K.V. (2010). Identification of host-dependent survival factors for intracellular *Mycobacterium tuberculosis* through an siRNA screen. *PLoS Pathog.* **6**, e1000839. <http://dx.doi.org/10.1371/journal.ppat.1000839>.
- Karnovsky, M. (1971). Use of ferrocyanide-reduced osmium tetroxide in electron microscopy. In *Proceedings of the Eleventh Annual Meeting of the American Society for Cell Biology*.
- Keane, J., Remold, H.G., and Kornfeld, H. (2000). Virulent *Mycobacterium tuberculosis* strains evade apoptosis of infected alveolar macrophages. *J. Immunol.* **164**, 2016–2020.
- Kimura, S., Noda, T., and Yoshimori, T. (2007). Dissection of the autophagosome maturation process by a novel reporter protein, tandem fluorescently-tagged LC3. *Autophagy* **3**, 452–460.
- Klionsky, D.J., Abeliovich, H., Agostinis, P., Agrawal, D.K., Aliev, G., Askew, D.S., Baba, M., Baehrecke, E.H., Bahr, B.A., Ballabio, A., et al. (2008). Guidelines for the use and interpretation of assays for monitoring autophagy in higher eukaryotes. *Autophagy* **4**, 151–175.
- Kobayashi, T., Stang, E., Fang, K.S., de Moerloose, P., Parton, R.G., and Gruenberg, J. (1998). A lipid associated with the antiphospholipid syndrome regulates endosome structure and function. *Nature* **392**, 193–197.
- Koul, A., Herget, T., Klebl, B., and Ullrich, A. (2004). Interplay between mycobacteria and host signalling pathways. *Nat. Rev. Microbiol.* **2**, 189–202.
- Kuijl, C., Savage, N.D., Marsman, M., Tuin, A.W., Janssen, L., Egan, D.A., Ketema, M., van den Nieuwendijk, R., van den Eeden, S.J., Geluk, A., et al. (2007). Intracellular bacterial growth is controlled by a kinase network around PKB/AKT1. *Nature* **450**, 725–730.
- Kumar, D., Nath, L., Kamal, M.A., Varshney, A., Jain, A., Singh, S., and Rao, K.V. (2010). Genome-wide analysis of the host intracellular network that regulates survival of *Mycobacterium tuberculosis*. *Cell* **140**, 731–743.
- Laplante, M., and Sabatini, D.M. (2012). mTOR signaling in growth control and disease. *Cell* **149**, 274–293.
- Matsuzawa, T., Kim, B.H., Shenoy, A.R., Kamitani, S., Miyake, M., and Macmicking, J.D. (2012). IFN- γ elicits macrophage autophagy via the p38 MAPK signaling pathway. *J. Immunol.* **189**, 813–818.
- Pieters, J. (2008). *Mycobacterium tuberculosis* and the macrophage: maintaining a balance. *Cell Host Microbe* **3**, 399–407.
- Ponpuak, M., Davis, A.S., Roberts, E.A., Delgado, M.A., Dinkins, C., Zhao, Z., Virgin, H.W., 4th, Kyei, G.B., Johansen, T., Vergne, I., and Deretic, V. (2010). Delivery of cytosolic components by autophagic adaptor protein p62 endows autophagosomes with unique antimicrobial properties. *Immunity* **32**, 329–341.
- Poser, I., Sarov, M., Hutchins, J.R., Hériché, J.K., Toyoda, Y., Pozniakovsky, A., Weigl, D., Nitzsche, A., Hegemann, B., Bird, A.W., et al. (2008). BAC

- TransgeneOmics: a high-throughput method for exploration of protein function in mammals. *Nat. Methods* 5, 409–415.
- Regenthal, R., Krueger, M., Koeppel, C., and Preiss, R. (1999). Drug levels: therapeutic and toxic serum/plasma concentrations of common drugs. *J. Clin. Monit. Comput.* 15, 529–544.
- Rink, J., Ghigo, E., Kalaidzidis, Y., and Zerial, M. (2005). Rab conversion as a mechanism of progression from early to late endosomes. *Cell* 122, 735–749.
- Rossi, M., Munarriz, E.R., Bartesaghi, S., Milanese, M., Dinsdale, D., Guerra-Martin, M.A., Bampton, E.T., Glynn, P., Bonanno, G., Knight, R.A., et al. (2009). Desmethylclomipramine induces the accumulation of autophagy markers by blocking autophagic flux. *J. Cell Sci.* 122, 3330–3339.
- Russell, D.G. (2001). *Mycobacterium tuberculosis*: here today, and here tomorrow. *Nat. Rev. Mol. Cell Biol.* 2, 569–577.
- Schmid, S.L., and Cullis, P.R. (1998). Membrane sorting. Endosome marker is fat not fiction. *Nature* 392, 135–136.
- Schwegmann, A., and Brombacher, F. (2008). Host-directed drug targeting of factors hijacked by pathogens. *Sci. Signal.* 1, re8.
- Seglen, P.O., and Gordon, P.B. (1982). 3-Methyladenine: specific inhibitor of autophagic/lysosomal protein degradation in isolated rat hepatocytes. *Proc. Natl. Acad. Sci. USA* 79, 1889–1892.
- Settembre, C., Di Malta, C., Polito, V.A., Garcia Arencibia, M., Vetrini, F., Erdin, S., Erdin, S.U., Huynh, T., Medina, D., Colella, P., et al. (2011). TFEB links autophagy to lysosomal biogenesis. *Science* 332, 1429–1433.
- Shubin, H., Sherson, J., Pennes, E., Glaskin, A., and Sokmensuer, A. (1958). Prochlorperazine (compazine) as an aid in the treatment of pulmonary tuberculosis. *Antibiotic Med. Clin. Ther.* 5, 305–309.
- Swinney, D.C., and Anthony, J. (2011). How were new medicines discovered? *Nat. Rev. Drug Discov.* 10, 507–519.
- Vergne, I., Chua, J., Lee, H.H., Lucas, M., Belisle, J., and Deretic, V. (2005). Mechanism of phagolysosome biogenesis block by viable *Mycobacterium tuberculosis*. *Proc. Natl. Acad. Sci. USA* 102, 4033–4038.
- Zschocke, J., Zimmermann, N., Berning, B., Ganai, V., Holsboer, F., and Rein, T. (2011). Antidepressant drugs diversely affect autophagy pathways in astrocytes and neurons—dissociation from cholesterol homeostasis. *Neuropsychopharmacology* 36, 1754–1768.